Physics of Plasmas

Neutralization of ion beam by electron injection: Accumulation of cold electrons

Cite as: Phys. Plasmas **27**, 043108 (2020); https://doi.org/10.1063/1.5128521
Submitted: 19 September 2019 . Accepted: 07 April 2020 . Published Online: 23 April 2020

C. Lan, and I. D. Kaganovich

Physics of Plasmas ARTICLE scitation.org/journal/php

Neutralization of ion beam by electron injection: Accumulation of cold electrons

Cite as: Phys. Plasmas **27**, 043108 (2020); doi: 10.1063/1.5128521
Submitted: 19 September 2019 · Accepted: 7 April 2020 ·
Published Online: 23 April 2020

View Online Export Citation CrossMark

C. Lan[1,2,a] and I. D. Kaganovich[2]

AFFILIATIONS

[1]Institute of Fluid Physics, China Academy of Engineering Physics, Mianyang 621900, People's Republic of China
[2]Princeton Plasma Physics Laboratory, Princeton, New Jersey 08543, USA

[a]Author to whom correspondence should be addressed: lanchaohui@163.com

ABSTRACT

Ion beam charge neutralization by electron injection is a complex kinetic process. Recent experiments show that the resulting self-potential of the ion beam after neutralization by plasma is much lower than the temperature of plasma electrons [Stepanov *et al.*, Phys. Plasmas **23**, 043113 (2016)], indicating that kinetic effects are important and may affect the neutralization of the ion beam. We performed a numerical study of the charge neutralization process of an ion beam making use of a two-dimensional electrostatic particle-in-cell code. The results show that the process of charge neutralization by electron injection is composed of two stages. During the first stage, the self-potential of the beam is higher than the temperature of injected electrons (T_e/e) and all injected electrons are captured by the ion beam. During the second stage, hot electrons escape from the ion beam and the beam self-potential (φ) decreases because cold electrons slowly accumulate resulting in the beam self-potential φ to become much lower than T_e/e in agreement with previous experimental observations at Princeton Advanced Teststand. We also determined that the resulting φ scales as $\varphi \sim \sqrt{T_e}$, in agreement with previous experimental observations from Gabovich's group. In addition, the results show that the transverse position of the electron source has a great impact on ion beam neutralization. A slight shift of the electron source as relevant to the ion thrusters leads to a large increase in the beam self-potential because of an increase in potential energy of injected electrons.

I. INTRODUCTION

Ion beams are widely used in many areas including accelerators,[1] ion thrusters,[2] inertial fusion, in particular fast ignition[3] and heavy ion fusion,[4] surface engineering,[5–11] etc. In surface engineering, ion beams are usually used for etching, deposition of thin films, and ion implantation. In addition, ion beams find applications in ion beam lithography and more recently nanopantography.[5] Many of these applications require intense ion beam pulses with strong space-charge forces. Because of intense self-electric fields of ion beams, effective neutralization of space charge is necessary to prevent defocusing and the decrease in ion beam flux, especially for low energy ion beams. For instance, a heavy ion fusion driver like NDCX can generate tens of amperes of ion current at MeV but requires near-complete (99%) space charge neutralization in order to produce a tight focus of the ion beam.[12–14] Space-charge compensation is also important for other ion beam applications, for example, for etching of insulators[6] and especially nanopantography.[5]

Space-charge compensation or neutralization of ion beams can reduce beam perveance by introducing electrons. This is different to the electron-cooling method,[15] which has been actively used in ion storage rings like LEAR,[16] RHIC,[17] SIS,[18] etc., to reduce beam emittance. The electron-cooling method is based on the cooling of ion beam perpendicular temperature in the Coulomb collisions of the ion beam and electron beam particles. The ion beam neutralization uses negatively charged electrons only to compensate the space charge of ion beams and transport or focus ion beams.

To compensate for a space charge potential of a positive ion beam, a sufficiently large number of electrons must be introduced from outside. This can be carried out by injecting electrons or producing plasma near or in the path of ion beam propagation, and it has been found that the neutralization degree of the ion beam is associated with the scheme of introducing electrons.[12] One simple way to inject electrons is to use hot filaments, which can emit electrons from filaments.[19,20] The temperature of emitted electrons is equal to the temperature of filaments and is about 0.1 eV. For a plasma source operated in a vacuum, the electron temperature is usually much higher than this value. However, it was experimentally shown in Ref. 20 that the ion beam pulse neutralization by filaments provides much poor

neutralization as compared with neutralization by plasmas. In our recent paper,[21] we reported that when an ion beam pulse passes through an electron-emitting filament, the generation of electrostatic solitary waves (ESWs) occurs due to the two-stream instability of neutralizing electrons. ESWs are well studied in different plasma systems[22–28] but it was only recently shown that they can form during the neutralization process of the ion beam pulse.[21] Moreover, it was observed in two-dimensional (2D) particle-in-cell (PIC) simulations that only ESWs can survive for a long time with the lifetime of about several microseconds and the generation of ESWs has a great impact on the degree of neutralization of the ion beam pulse.

Possible excitation of ESWs can provide an explanation of why past experimental studies showed poorer ion beam neutralization by filaments compared with neutralization by plasmas. The detailed description of the excitation of ESWs will be presented in Ref. 29. In this paper, we consider only long beam pulses (longer than several microseconds) when ESWs disappear and cold electrons accumulate and substantially reduce the beam self-potential. Long-distance propagation of long ion beam pulses requires very small residual space charges. Note that numerous previous studies did not address this issue and were limited by simulation of much shorter beam pulses, as introduced below.

In Ref. 13, the authors reported experiments on ion beam neutralization by a ferroelectric plasma source. This type of plasma source can provide 1–2 eV electrons by surface discharge. However, the experimental results show that the transverse electrostatic potential (~0.3 V) of the neutralized ion beam is much lower than the electron temperature, implying that the energy of the neutralizing electrons was below 0.3 eV. Such a low temperature can be explained as follows. With the decay of space charge potential of the ion beam during neutralization, fast electrons can escape from the formed potential well, while cold electrons continuously accumulate inside the ion beam. This is similar to processes in glow dc discharge leading to the formation of negative glow with nearly room temperature electrons.[30,31] In this paper, we simulate the process of neutralization with filaments and show similar phenomena. The fact that we use filament as a source of electrons makes no difference in physics but allows for fast simulations.

In Refs. 32 and 33, it was experimentally shown that the neutralization degree or the beam self-potential depends on the electron temperature inside the ion beam. Here, the beam self-potential is defined as the electric potential on the axis of the beam relative to the grounded walls; it varies with the neutralization degree. In the experiments, authors of Refs. 32 and 33 studied the process of beam neutralization through residual gas ionization and confirmed that Coulomb collisions of beam ions with neutralizing electrons provide an energy source for heating of captured electrons. In this paper, we simulate the process of neutralization with filaments and show similar phenomena that the resulting self-potential depends on the electron temperature in a non-trivial manner.

Ion beam neutralization and propagation have been modeled and studied by many researchers in the past twenty years. For completeness, we briefly summarize these studies. Welch *et al.*[34] and Rose *et al.*,[35] investigated three different propagation schemes of heavy ion beams using 2D LSP and 3D IPROP codes. Background gas ionization, as well as electron emission from conducting surfaces, was modeled in their simulations. In Ref. 36, they numerically studied ion beam scatter caused by small charge clumps in the beam. Using the 2D WARP code, de Hoon *et al.*[37] performed particle-in-cell (PIC) simulations of the beam dynamics of the scaled final focus system. Sefkow *et al.*,[38] used a 3D hybrid kinetic-fluid LSP code to study the spatial and temporal evolution of plasma parameters for two types of sources used in the NDCX. The background plasma density and temperature were varied and the neutralization and beam potential were analyzed in this paper. In Refs. 39 and 40, the electromagnetic Weibel and electrostatic two-stream instabilities were investigated analytically and numerically for an intense ion beam propagating through a background plasma. Kaganovich *et al.*[12,41–43] used LSP and fluid codes to systematically study the effects of different neutralization schemes on the ion beam neutralization process. They discussed the excitation of collective plasma waves during neutralization, the effects of gas ionization, finite electron temperature, and applied solenoidal and dipole magnetic fields. Also Berdanier *et al.*[44] performed PIC simulations with the LSP code to show the advantage of ion beam neutralization using underdense background plasma and compared simulation results with experimental data from the NDCX.

However, none of the previous numerical studies observed the effects of electron accumulation and resulting excitation of ESWs in sufficiently long beam pulses because it requires simulations with very good resolution and long simulation time, which was not performed earlier.

In addition, previous authors did not consider the influence of the way of introducing electrons on the behavior of electrons inside the ion beam. This is particularly important for the neutralization of ion beams by hot filaments and especially for electric propulsion devices.[45,46] Because in this case the injector location is restricted to be outside of the beam, the neutralizing electrons must move into the beam to neutralize. As a result, the neutralization process and the behavior of neutralizing electrons are much more complicated compared with the neutralization through gas ionization or plasma injection. Accumulation and motion of electrons in the potential well formed by the beam are complicated and the resulting velocity distribution function of neutralizing electrons is anisotropic and sufficiently different from Maxwellian distribution, which is the subject of this paper.

In this paper, we focus on the kinetic effects of neutralizing electrons, especially the motion of neutralizing electrons with different energies inside or outside the ion beam. To focus on the physical processes rather than on technical details of previous experiments, an idealized model (without background gas ionization and secondary electron emission) of ion beam neutralization was employed, and the behavior of electrons was numerically investigated using a 2D PIC code. The code is a 2D generalization of 1D implicit code EDIPIC[47–49] and our simulations resolve the Debye length and plasma frequency. In this paper, we mainly study the accumulation process of cold electrons and its influence on the neutralization of ion beams. The detailed description of the resulting excitation of ESWs during the accumulation of cold electrons will be presented in Ref. 29.

The paper is organized as follows: in Sec. II, a 2D simulation model of ion beam neutralization by injecting electrons is described. The simulation results and corresponding discussion are given in Sec. III. Conclusions are summarized in Sec. IV.

II. SIMULATION MODEL

The 2D setup shown in Fig. 1 was used to simulate the ion beam transport in a metal pipe. Electrons are injected on the axis to

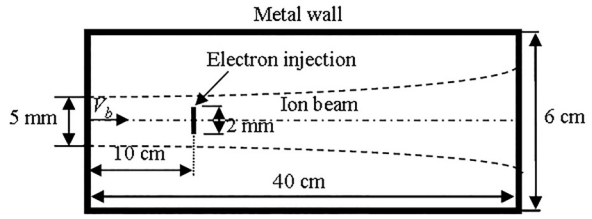

FIG. 1. Schematic of the simulation model. The model is 2D in the *x*-*y* Cartesian coordinate system. The ion beam moves along the axis of the model with speed V_b. Electrons are injected on the axis. Dashed curves represent the envelope of the ion beam.

neutralize the ion beam. Ion beam, electron injection, and transporting metal pipe comprise a simple but complete physical model of neutralization. Such an electron injection scheme represents the electron emission by hot filaments placed into the beam path.[19] For simplicity, the model is 2D in an *x*-*y* uniform Cartesian coordinate system, where *x* is in the direction of ion beam propagation and *y* is the transverse direction. The size of the computational domain is 40 cm × 6 cm. The cell size of a uniform Cartesian grid is 0.25 mm, which leads to a grid of 1600 × 240 cells.

Monoenergetic Ar^+ (atomic mass 39.95) beam with ion current $I_b = 0.06$ A/m, energy $E_b = 38$ keV, and beam width $L_b = 5$ mm is uniformly injected into the initially empty domain from the center of the left boundary. The flow velocity of ion V_b is about 42.7 cm/μs. So the initial density of the ion beam is $n_b = I_b/q_e V_b L_b \approx 1.75 \times 10^{14}$ m^{-3}, where q_e is the electron charge. These parameters of the ion beam are chosen close to those of Princeton Advanced Test Stand at PPPL.[13] Because ion beam current is very low and the flow velocity of the ion beam V_b satisfies $V_b \ll c$, where c is the light speed, the inductive magnetic field of the ion beam in a vacuum can be neglected compared to its self-electric field, and the system can be treated electrostatically. Therefore, in 2D PIC simulations, Poisson's equation was used to obtain the electric potential from charge density.

The time step of the simulations is 80 ps. In order to reduce numerical noise and numerical heating, about 3500 macro-particles per cell are employed to represent the ion beam with density $n_b \approx 1.75 \times 10^{14}$ m^{-3}. That is, about 9600 macro-particles of ion are injected per time step. Every macro-particle represents 3125 true particles in the 2D case. After propagating for about 1 μs with fixed ion current, the ion beam reaches the right wall. Then electrons start to be injected at 1 μs. The position of the injection is on the path of the ion beam ($x = 10$ cm). The width of the electron injector is 2 mm in the *y* direction, while no size in the *x* direction. In order to inhibit excitation of various plasma waves or instabilities, injected electron current (or the number of electrons injected per time step) should be sufficiently small, with 1/3 of ion beam current in our simulation setup. That is, about 3200 macro-particles of electron are injected per time step. To study a wider range of physical laws, the electron temperature is not limited to the typical temperature of hot filaments and varied within several electron volts.

Upper and lower metal walls are totally absorbing boundaries for particles. For left and right boundaries, considering that in experiments ion beams are usually extracted through a metal grid, and collected by a Faraday cup or directly hit a metal target after traveling a distance, so both left and right walls of the model can be treated as metal boundaries for electric field and absorbing boundaries for particles. When ions hit a metal wall, a great number of secondary electrons will be created. However, these electrons will oscillate many times in the potential well formed by the ion beam. As a result, thermalizing and cooling these electrons require a much longer timescale. So, for simplicity, ion-induced secondary electron emission was not considered in our simulations.

The collisions between charged particles and neutral particles were not modeled and Coulomb collisions between charged particles were also neglected as they only weakly affect the neutralization process. A single simulation lasted for more than 30 μs. Simulations were run with 40 cores on the Princeton University Adroit supercomputer.

III. RESULTS AND DISCUSSION

A. Accumulation of cold electrons during ion beam neutralization

The injected ion beam is perfectly collimated with zero divergence, so that the expansion of the ion beam is only determined by the remaining space charge and the beam envelope $R(x)$ is described by the perveance Q of the ion beam

$$\frac{\partial^2 R}{\partial x^2} = \frac{(1-f)Q}{R}, \tag{1}$$

where f is the neutralization fraction of the ion beam.

Figure 2 shows the evolution of particle density profiles during the neutralization of the ion beam. As seen from this figure, the initially expanding ion beam gradually shrinks in envelope after the neutralization begins. According to the downstream divergence angle and the width of the ion beam, one can calculate from Eq. (1) that the neutralization fraction has reached more than 99% at $t = 4.3$ μs. Because of the very deep potential well, electrons initially are distributed near the axis of the ion beam. As the neutralization fraction increases, electrons gradually fill up the whole ion beam and some of the hot electrons escape the potential well and get lost on the walls.

If we do not consider the loss of hot electrons, the time required to completely neutralize ions is determined by

$$\Delta t = \frac{I_i L}{I_e}\sqrt{\frac{2m_i}{E_b}}, \tag{2}$$

where I_i and I_e are the currents of the ion beam and injected electrons, respectively. L is the length of the ion beam and m_i is the ion mass. In this simulation, we have $I_i/I_e = 3$; therefore, $\Delta t = 3.2$ μs. However, because of the loss of hot electrons, the time required to neutralize ions is longer than this value.

Figure 3 plots the temporal evolution of the beam potential on the axis and the neutralization fraction of the ion beam. The ion beam potential reaches a steady state at around 1 μs. As electrons are continuously injected into the ion beam, the beam potential is decreased almost linearly from a maximal value of about 220 V. After around $\Delta t = 2.8$ μs, i.e., $t \approx 3.8$ μs, the beam potential curve as a function of time reaches an inflexion point. At this point, the attainable neutralization fraction is 98% and the beam potential is about 4 V, which is twice the temperature of injected electrons, $T_e = 2$ eV for this case. After that, the neutralization of the ion beam enters the second stage. Hot electrons with energies larger than the beam potential could escape from the potential well; meanwhile, more and more cold electrons are

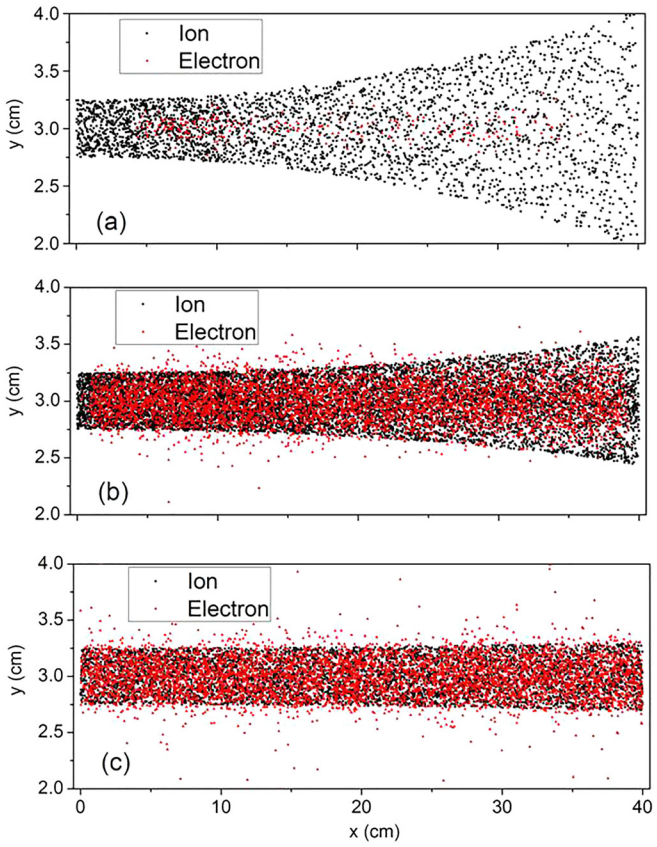

FIG. 2. Spatial distributions of electrons and ions at (a) $t = 1.2$ μs, (b) $t = 3.2$ μs, and (c) $t = 4.3$ μs. The temperature of injected electrons is $T_e = 2$ eV.

being trapped in this potential well, causing the beam potential to continue to decline. As a result, the minimum residual potential of the ion beam is far below the temperature of injected electrons, as shown in Fig. 3. This is a very slow dynamic process. After this stage, the neutralization fraction is increased from 98% to more than 99%. As the beam potential decreases, electrons inside the ion beam become colder and colder, until reaching a particle balance that the rate of capture of cold electrons is equal to the rate at which cold electrons are heated and escaped.

In Fig. 3, we can see that the second stage of neutralization is very important. Without this stage, a 99% neutralization fraction is hard to obtain. For the case of T_e/e $\varphi_0 > 1\%$, where T_e is the temperature of injected electrons and φ_0 is the beam potential before neutralization, in order to get over a 99% neutralization fraction, the accumulation of cold electrons is necessary.

It should be noted that the occurrence of the second stage of neutralization does not rely on the single point electron injection, and even does not rely on the injection location of electrons (see Fig. 10 below). As long as electrons are continuously generated near the potential well of the ion beam, the accumulation of cold electrons will occur.

The ultimate residual potential of the ion beam is determined by many factors such as Coulomb collisions between charged particles

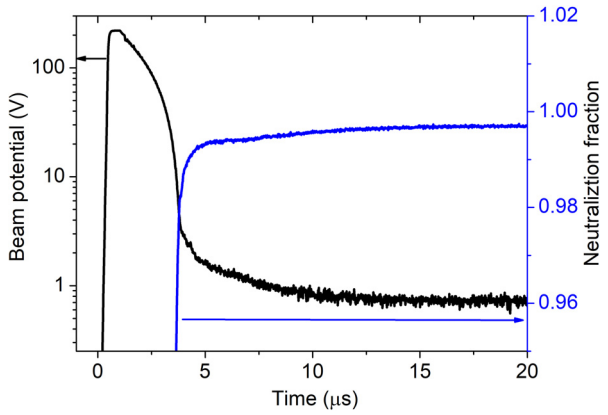

FIG. 3. Temporal evolutions of the beam potential at $x = 20$ cm and the neutralization fraction of the ion beam. Beam potential φ is defined as the potential on the axis of the beam. The neutralization fraction is obtained via φ/φ_0, where φ_0 is the beam potential without neutralization.

(not included in this model),[32] wave-particle interaction, the influence of electron source and numerical heating caused by macro-particle and spatial gridding of the PIC method,[50] etc. The study of these heating mechanisms of cold electrons is beyond the scope of this paper. We focus our attention on the behavior of cold electrons before reaching the particle balance. It can be seen in Fig. 3 that the second stage, i.e., accumulation of cold electrons, can last for more than 15 μs. The residual potential of the ion beam we can obtain from this simulation is close to 0.7 V, which is about twice the measured residual potential in Ref. 13. The difference may be due to the different ways in which electrons are injected and numerical heating that does not exist in experiments.

Because the temperature of cold electrons is finite and the neutralization degree of the ion beam is close to 1, some of the cold electrons are located outside the ion beam. Consequently, the distribution of electrons outside the ion beam leads to the generation of a radial electric field. Figure 4 shows the distributions of particle densities in the y direction at different moments. At the beginning of the neutralization,

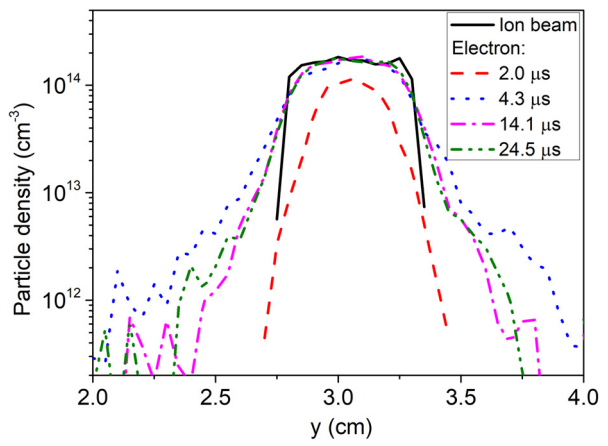

FIG. 4. Distributions of the electron density and the ion density along the y direction at different moments ($x = 20$ cm).

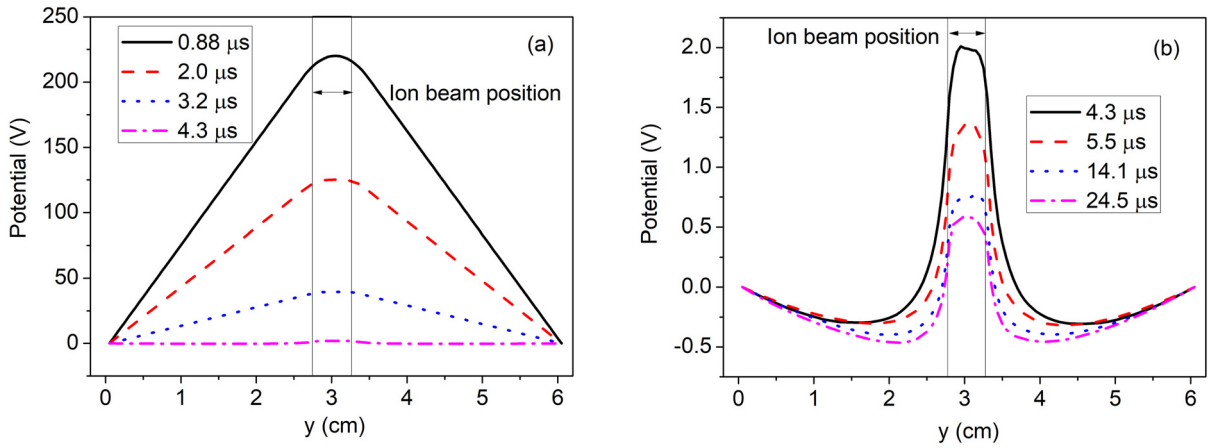

FIG. 5. Distribution of the potential along the y direction ($x = 20$ cm) at different moments, (a) t is from 0.88 μs to 4.3 μs and (b) t is from 4.3 μs to 24.5 μs.

all the injected electrons are located inside the ion core. When the beam potential is reduced to several volts, a large number of hot electrons start spilling out. As electrons captured by the ion beam get colder, the number of electrons distributed outside the ion beam becomes smaller.

The profiles of potential along the y direction at different moments of time are shown in Fig. 5. Figures 5(a) and 5(b), respectively, corresponding to the first and the second stages of neutralization. We can see clearly how the potential well evolves in the whole process of neutralization. Because of the 2D model, at the first stage, the potential outside the ion beam is linearly decreased with the transverse distance from the ion beam and linearly decreased with time. However, at the second stage because of the distribution of electrons outside the ion beam, the actual depth of the potential well is larger than the beam potential, implying that the kinetic energy of cold electrons can be larger than the beam potential at that moment. Furthermore, the colder electrons accumulate, the greater the deviation. This result does not contradict the conclusion of Ref. 13, because of different ways of introducing electrons. In the experimental studies in Ref. 13, electrons were generated on the surface of the outer wall. But here electrons are directly injected into the center of the ion beam.

The accumulation of cold electrons and the depletion of hot electrons can be clearly seen through the evolution of electron velocity distribution functions (EVDFs), which are presented in Fig. 6. About 4 μs later, hot electrons begin to escape. But the accumulation of cold electrons has been going on since the beginning of electron injection. Due to the fact that the scale of potential well formed by the ion beam varies greatly in different directions, the behavior of neutralizing electrons exhibits anisotropy during neutralization. When electrons are injected into the center of the ion beam, cold electrons tend to drift along the x direction under the action of a longitudinal electric field. This longitudinal electric field is caused by the space charge near the

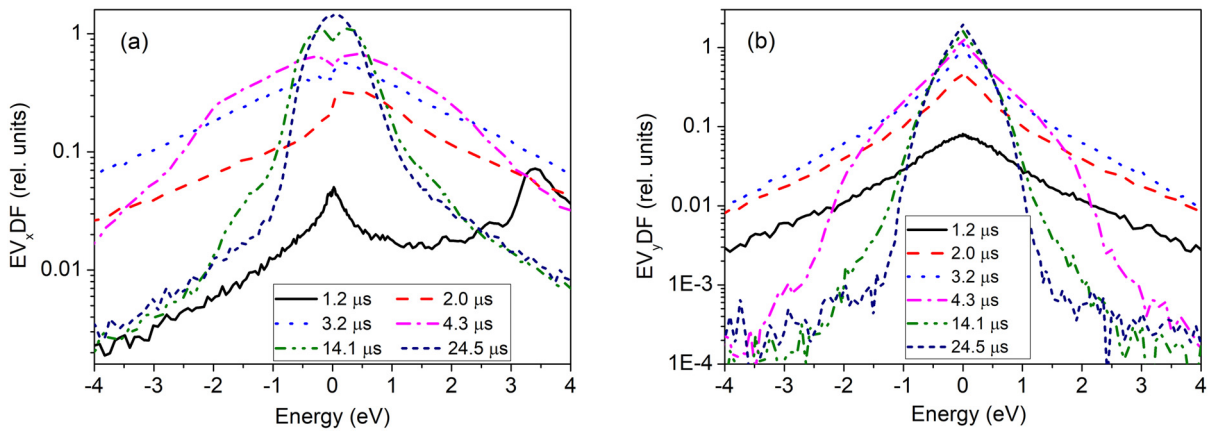

FIG. 6. Temporal evolutions of EV_xDF and EV_yDF. The EV_xDF is defined as $\int_{-\infty}^{+\infty} f(v_x, v_y, v_z)dv_y v_z$, f is the electron velocity distribution function (EVDF). All electrons in the domain are taken into account, but electrons outside the ion beam take up a very small portion. The distribution functions are plotted in energy coordinates; negative energy values correspond to propagation in a negative direction. The asymmetry of EV_xDF is caused by the spatial asymmetry of electron injection. In the logarithmic coordinate system, the Maxwellian velocity distribution with the initial electron temperature of 2 eV is two straight lines. So the EV_yDF before 3 μs shown in (b) is basically close to the Maxwellian distribution.

location of electron injection. If the energies of cold electrons are below the beam potential, they will bounce back into the ion beam from the left and right walls, forming two streams of cold electrons moving in the opposite direction with comparable densities, as shown in Fig. 6(a). However, this phenomenon is not observed in the y direction. The EV_yDF is basically close to the Maxwellian distribution before 3 μs and in the range of low energy (<0.5 eV) of all time. The reason may be due to a much smaller scale of the potential well in the y direction ($\sim$1 cm in the y direction vs 40 cm in the x direction). As a result, the transverse motion of cold electrons is effectively restrained.

The double-peak EV_xDF shown in Fig. 6(a) not only appears at the beginning of the electron injection ($t = 1.2$ μs) but also appears at the second stage of beam neutralization, indicating that the plasma composed of the ion beam and neutralizing electrons is unstable. Subsequent evolution will be discussed in the last part of this series. As more and more cold electrons accumulate in the potential well, we see that the double-peak EV_xDF gradually disappears and the EV_xDF tends to be Maxwellian.

B. Scaling of beam potential with the temperature of injected electrons

In Ref. 32, it has been found experimentally that the measured potential drop $\Delta\varphi$ from the center of the beam to the beam periphery has the following relation:

$$\Delta\varphi = C\sqrt{\Delta\varphi_0 T_e/e}, \tag{3}$$

where $\Delta\varphi_0$ is the potential drop of the un-neutralized ion beam and C is a coefficient whose value depends on the beam profile and applied electron source. T_e is the temperature of hot emitters, which is usually assumed to be equal to the temperature of emitted electrons. For the correlation between $\Delta\varphi$ (or beam potential φ, with a difference in coefficient for a given profile of ion beam) and T_e, we still lack sufficient numerical studies.[12] In this section, simulations were carried out to test the validity of this scaling relation.

In simulations, T_e was changed from 2 eV to 6 eV, while other parameters kept the same. Figure 7 shows how the beam potential changes with the temperature of injected electrons. Because T_e is still far smaller than the initial beam potential, we see in Fig. 7 that T_e does not affect the neutralization of the first stage. At the second stage of neutralization, as expected, higher electron temperature leads to slower accumulation of cold electrons. For the big hump that appeared in beam potential when $T_e = 6$ eV, it is caused by the ESWs.[29] The hump (and the peaks shown in Fig. 10) finally will disappear as the distribution of accumulated electrons tends to become Maxwellian. Therefore, the appearance of these peaks will not affect the general conclusions of this paper.

The beam potentials at arbitrary three moments of the second stage are plotted with respect to $\sqrt{T_e}$ in Fig. 8. Here, the abrupt change of beam potential caused by the ESWs is neglected. A near linear correlation between the beam potential and $\sqrt{T_e}$ can be clearly seen. As per Eq. (3), the beam potential should scale as $\varphi \sim \sqrt{T_e}$. This is demonstrated in Fig. 8 and consistent with experimental observations.[32]

C. Influence of injection position on ion beam neutralization

In previous numerical simulations, electrons were injected on the path of the ion beam, i.e., the lowest point of potential well of the ion beam. In this case, neutralizing electrons can gradually fill this potential well until they start to escape and collective processes for transverse electron motion are not observed. Nevertheless, if electron injection is shifted from the axis of the ion beam, the neutralization process of the ion beam will be quite different. In order to clearly show the effect of the injection position, we positioned the electron source far away ($y = 1$ mm) from the ion beam. Figure 9 plots the spatial distributions of ions and electrons at two moments, i.e., $t = 1.15$ μs and $t = 10$ μs. $t = 1.15$ μs corresponds to the first stage of neutralization, while $t = 10$ μs corresponds to the stable second stage of neutralization. In this case, we see from Fig. 9(a) that besides the motion in the beam propagation direction, electrons emitted from the box edge experience great transverse oscillation around the ion beam. Due to higher transverse acceleration, electrons constantly overshot the ion beam center and bounce between two edges, thus decreasing their residence time within the ion beam. Some electrons are thermalized through

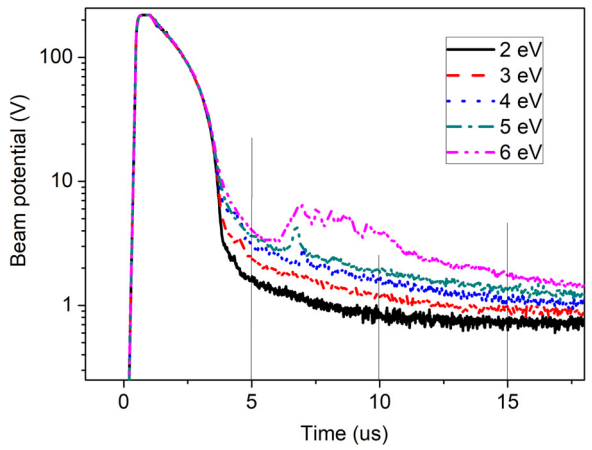

FIG. 7. Temporal evolutions of the beam potential for different temperatures of injected electrons. The peaks appeared on the curves are caused by the ESWs.

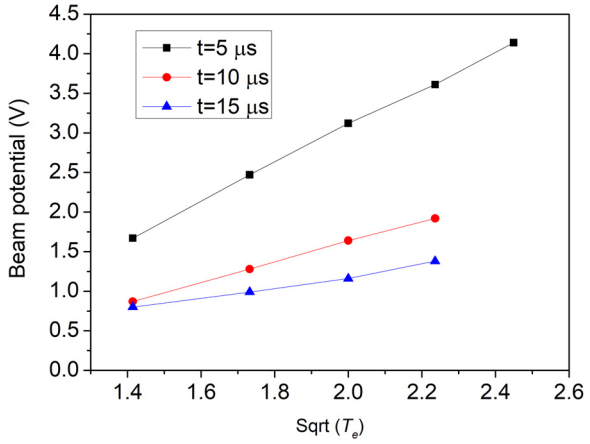

FIG. 8. Scaling relation between the beam potential and the temperature of injected electrons at different moments.

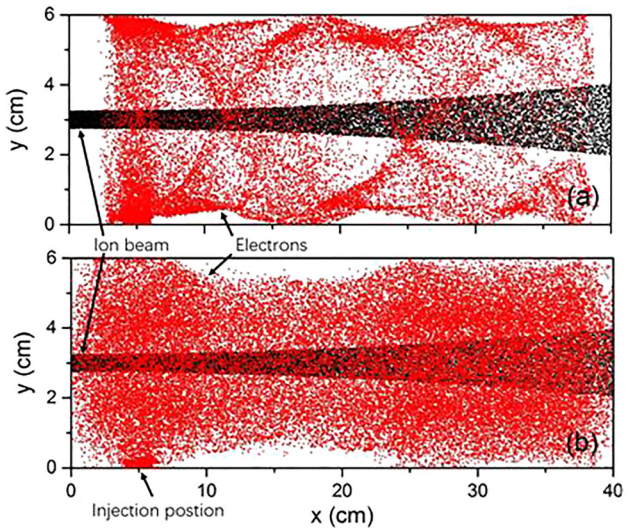

FIG. 9. Oscillation of neutralizing electrons around the ion beam when electron injection is shifted from the beam axis. (a) $t = 1.15$ μs and (b) $t = 10$ μs. Electrons start to be injected at $t = 1$ μs.

electron–electron two-stream instability and reside in the ion beam, but this process is very slow. Consequently, the neutralization degree of the ion beam is very low, and the self-consistent electric field causes the ion beam to undergo defocusing, as shown in Fig. 9(b).

We varied the position of the electron source in simulation to investigate its influence on ion beam neutralization. Figure 10 shows the temporal evolution of the beam potential during ion beam neutralization, four curves corresponding to four positions of electron injection. The peaks that appeared at about 5 μs are due to the excitation of small-amplitude ESWs and they will finally disappear. It is evidently seen that slight alteration of the electron source in the y direction (from 0 to 5 mm) leads to an order of magnitude increase in beam

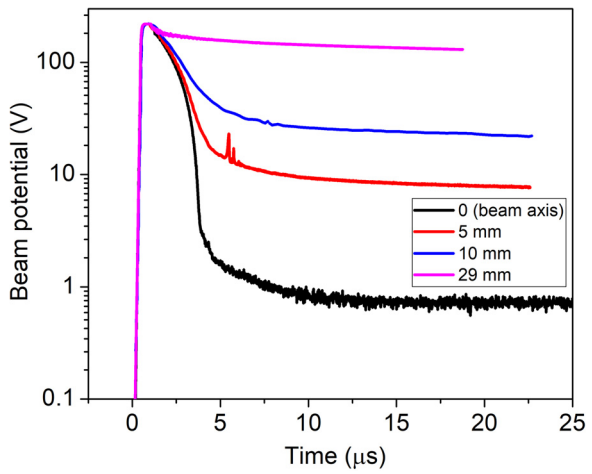

FIG. 10. Influence of the position of electron injection on the beam potential during ion beam neutralization. 5 mm, 10 mm, and 29 mm are distances from the beam axis. The peaks at about $t = 5$ μs are caused by the ESWs.

self-potential, thereby resulting in much higher beam potential than the temperature of injected electrons. Therefore, the neutralization of the ion beam is very sensitive to the transverse position of the electron source. When the electron injector is close to the bottom boundary, the beam potential reaches more than 150 V, indicating a very low degree of neutralization of the ion beam. It is worth noting that the two-stage neutralization process mentioned above still exists for an electron source shifted to the periphery, and the turning point between two stages almost keeps unchanged (except for a very large shift distance). Meanwhile, in the logarithmic coordinates, the slope of decline after 7.5 μs is nearly the same for a relatively larger shift of the electron source, indicating that even though very slow, the accumulation of electrons inside the ion beam causes an exponential decline of the beam self-potential.

IV. CONCLUSIONS

In this paper, we have presented 2D particle-in-cell numerical studies of the neutralization of an ion beam by electron injection. The simulation results show that the neutralization process is composed of two stages. At the first stage, due to the high potential well, almost all electrons can be captured by the ion beam, leading to the rapid decline of the beam self-potential. At the second stage, cold electrons are slowly accumulated while hot electrons with energies higher than the beam potential are escaped from the potential well. The second stage takes a much longer time than the first stage and the resulting beam self-potential becomes far less than the electron temperature of the source. Without the second stage of neutralization, the neutralization degree will not exceed 99%. Our numerical simulations confirm that the residual potential linearly scales as $\sqrt{T_e}$ at different moments during the accumulation of cold electrons, where T_e is the temperature of injected electrons. In the process of cold electron accumulation, because there is a big difference in the size of potential well in both directions, the electron distribution function exhibits some anisotropy. Double-peak EV_xDF appeared at the second stage of neutralization indicates that cold electron EVDFs are unstable due to the two-stream instability. In addition, the neutralization process of the ion beam is very sensitive to the transverse position of the electron source. A transverse shift of the electron source from the center to the periphery makes cold electrons accumulate more slowly, thus reducing the neutralization degree of the ion beam.

ACKNOWLEDGMENTS

The work of Igor D. Kaganovich was supported the by U.S. Department of Energy. The work of Chaohui Lan was supported by the International Cooperation and Exchange Fund of China Academy of Engineering Physics.

REFERENCES

[1]P. Chen, J. M. Dawson, R. W. Huff, and T. Katsouleas, Phys. Rev. Lett. **54**, 693 (1985); R. Govil, W. P. Leemans, E. Y. Backhaus, and J. S. Wurtele, *ibid.* **83**, 3202 (1999).
[2]S. Humphries, Appl. Phys. Lett. **32**, 792 (1978).
[3]A. J. Kemp, W. P. Leemans, E. Y. Backhaus, and J. S. Wurtele, Phys. Rev. Lett. **97**, 235001 (2006); R. J. Mason, *ibid.* **96**, 035001 (2006).
[4]P. K. Roy, S. S. Yu, E. Henestroza, A. Anders, F. M. Bieniosek, J. Coleman, S. Eylon, W. G. Greenway, M. Leitner, B. G. Logan *et al.*, Phys. Rev. Lett. **95**, 234801 (2005); B. G. Logan, F. M. Bieniosek, C. M. Celata, J. Coleman, W.

Greenway, E. Henestroza, J. W. Kwan, E. P. Lee, M. Leitner, P. K. Roy *et al.*, Nucl. Instrum. Methods Phys. Res., Sect. A **577**, 1 (2007).
[5]J. P. Chang, J. C. Arnold, G. C. H. Zau, H.-S. Shin, and H. H. Sawin, J. Vac. Sci. Technol., A **15**, 1853–1863 (1997).
[6]A. Stojkovic, M. Radmilovic-Radenovic, and Z. L. Petrovic, Mater. Sci. Forum **494**, 297–302 (2005).
[7]M. Watanabe, D. M. Shaw, and G. J. Collins, Appl. Phys. Lett. **79**, 2698 (2001).
[8]J. Ishikawa, H. Tsuji, K. Shibutani, H. Ikai, and Y. Gotoh, in Proceeding of 1998 International Conference on Ion Implantation Technology (1998), pp. 716–719.
[9]C. Fusellier, L. Wartski, J. Aubert, C. Schwebel, Ph. Coste, and A. Chabrier, Rev. Sci. Instrum. **69**, 1153 (1998).
[10]I. G. Brown and J. Washburn, Nucl. Instrum. Methods Phys. Res., Sect. B **21**, 201 (1987).
[11]L. Dumas, E. Quesnel, J.-Y. Robic, and Y. Pauleau, Thin Solid Films **382**, 61 (2001).
[12]I. D. Kaganovich, R. C. Davidson, M. A. Dorf, E. A. Startsev, A. B. Sefkow, E. P. Lee, and A. Friedman, Phys. Plasmas **17**, 056703 (2010).
[13]A. D. Stepanov, E. P. Gilson, L. R. Grisham, I. D. Kaganovich, and R. C. Davidson, Phys. Plasmas **23**, 043113 (2016).
[14]A. D. Stepanov, J. J. Barnard, A. Friedman, E. P. Gilson, D. P. Grote, Q. Ji, I. D. Kaganovich, A. Persaud, P. A. Seidl, and T. Schenkel, Matter Radiat. Extremes **3**, 78–84 (2018).
[15]G. I. Budker and A. N. Skrinskii, Sov. Phys. Usp **21**, 277 (1978).
[16]J. Bosser, M. Chanel, R. Ley, and G. Tranquille, in Proceedings of 1992 European Particle Accelerator Conference (1992), Vol. 1, p. 845.
[17]I. Ben-Zvi, L. Ahrens, M. Brennan, M. Harrison, J. Kewisch, W. MacKay, S. Peggs, T. Roser, T. Satogata, D. Trbojevic *et al.*, in Proceedings of 2001 Particle Accelerator Conference (2001), Vol. 1, p. 48.
[18]M. Steck, L. Groening, K. Blasche, B. Franczak, B. Franzke, T. Winkler, and V. V. Parkhomchuk, Nucl. Instrum. Methods Phys. Res., Sect. A **441**, 175 (2000).
[19]D. V. Rose, D. R. Welch, and S. A. MacLaren, in Proceedings of the 2001 Particle Accelerator Conference (2001), Vol. 3003.
[20]S. A. MacLaren, A. Faltens, and P. A. Seidl, Phys. Plasmas **9**, 1712 (2002).
[21]C. Lan and I. D. Kaganovich, Phys. Plasmas. **26**, 050704 (2019).
[22]R. L. Morse and C. W. Nielson, Phys. Rev. Lett. **23**, 1087 (1969).
[23]H. L. Berk, C. E. Nielsen, and K. V. Roberts, Phys. Fluids **13**, 980 (1970).
[24]H. Schamel, Phys. Scr. **20**, 336 (1979).
[25]H. Schamel, Plasma Phys. **13**, 491 (1971); **14**, 905 (1972).
[26]H. Schamel, Phys. Plasmas **7**, 4831 (2000).
[27]I. H. Hutchinson, Phys. Plasmas **24**, 055601 (2017).
[28]H. Matsumoto, H. Kojima, T. Miyatake, Y. Omura, M. Okada, I. Nagano, and M. Tsutsui, Geophys. Res. Lett. **21**, 2915, https://doi.org/10.1029/94GL01284 (1994).
[29]C. Lan and I. D. Kaganovich, "Neutralization of ion beam by electron injection: Excitation and propagation of electrostatic solitary waves," Phys. Plasmas **27**, 043104 (2020).
[30]L. D. Tsendin, Plasma Sources Sci. Technol. **12**, s51–s56 (2003).
[31]V. A. Rozhansky and L. D. Tsendin, *Transport Phenomena in Partially Ionized Plasma* (CRC Press, 2001).
[32]M. D. Gabovich, I. A. Soloshenko, and A. A. Ovcharenko, Ukr. Fiz. Zh. **15**, 934 (1971).
[33]I. A. Soloshenko, Rev. Sci. Instrum. **67**, 1646 (1996).
[34]D. R. Welch, D. V. Rose, B. V. Oliver, T. C. Genoni, R. E. Clark, C. L. Olson, and S. S. Yu, Phys. Plasmas **9**, 2344 (2002).
[35]D. V. Rose, D. R. Welch, B. V. Oliver, R. E. Clark, W. M. Sharp, and A. Friedman, Nucl. Instrum. Methods Phys. Res., Sect. A **464**, 299 (2001).
[36]C. L. Olson, D. L. Hanson, J. W. Poukey, and D. R. Welch, Fusion Eng. Des. **32-33**, 485 (1996).
[37]M. J. L. de Hoon, S. A. MacLaren, and E. P. Lee, Nucl. Instrum. Methods Phys. Res., Sect. A **464**, 278 (2001).
[38]A. B. Sefkow, R. C. Davidson, and E. P. Gilson, Phys. Rev. Spec. Top.-Accel. Beams **11**, 070101 (2008).
[39]R. C. Davidson, I. D. Kaganovich, E. A. Startsev, H. Qin, M. Dorf, A. Sefkow, D. R. Welch, D. V. Rose, and S. M. Lund, Nucl. Instrum. Methods Phys. Res., Sect. A **577**, 70 (2007).
[40]E. A. Startsev and R. C. Davidson, Nucl. Instrum. Methods Phys. Res., Sect. A **577**, 79 (2007).
[41]I. D. Kaganovich, G. Shvets, E. A. Startsev, and R. C. Davidson, Phys. Plasmas **8**, 4180 (2001).
[42]I. D. Kaganovich, E. Startsev, and R. C. Davidson, Phys. Plasmas **11**, 3546 (2004).
[43]I. D. Kaganovich, E. A. Startsev, A. B. Sefkow, and R. C. Davidson, Phys. Rev. Lett. **99**, 235002 (2007).
[44]W. Berdanier, P. K. Roy, and I. Kaganovich, Phys. Plasmas **22**, 013104 (2015).
[45]B. Korkut, Z. Li, and D. Levin, IEEE Trans. Plasma Sci. **43**, 1706–1721 (2015).
[46]B. Korkut and D. Levin, J. Propul. Power **33**, 264–212 (2017).
[47]D. Sydorenko, A. Smolyakov, I. Kaganovich, and Y. Raitses, Phys. Plasmas **13**, 014501 (2006).
[48]D. Sydorenko, Ph.D. thesis, University of Saskatchewan, 2006.
[49]M. D. Campanell, A. V. Khrabrov, and I. D. Kaganovich, Phys. Rev. Lett. **108**, 235001 (2012).
[50]H. Ueda, Y. Omura, H. Matsumoto, and T. Okuzawa, Comput. Phys. Commun. **79**, 249–259 (1994).